Journal of Materials Chemistry B

Accepted Manuscript

ROYAL SOCIETY OF CHEMISTRY

www.rsc.org/materialsB

Journal of
Materials Chemistry B
RSCPublishing

ARTICLE

Cite this: DOI: 10.1039/x0xx00000x

Water-Soluble Hyaluronic Acid-Hybrided Polyaniline Nanoparticles for Effectively Targeted Photothermal Therapy

Received 00th January 2014,
Accepted 00th January 2014

DOI: 10.1039/x0xx00000x

www.rsc.org/

Bang-Ping Jiang,‡ Li Zhang,‡ Yang Zhu, Xing-Can Shen* , Shi-Chen Ji, Xue-You Tan, Lei Cheng and Hong Liang*

The construction of advanced phototherapy systems with high therapeutic efficacy and low side effect toward cancer, especially targeted species, is highly desirable. Herein, we developed one kind of water-soluble hyaluronic acid-hybrided polyaniline nanoparticles (HA-PANI NPs) as a nanoplatform for photothermal therapy (PTT) with targeted specificity of CD44-mediated cancer cell. The water-soluble HA-PANI NPs were fabricated by one-step oxidative polymerization using aniline as polymerizable monomer and HA as a stabilizer and targeted agent, where non-covalently electrostatic interaction between the negatively charged polymer HA and the cationic polymer PANI drives the formation of HA-PANI NPs. It was demonstrated that approximately spherical HA-PANI NPs are well-dispersed in aqueous solutions, with average hydrodynamic diameter around 100 nm. Besides, HA-PANI NPs have negligible cytotoxicity *in vitro*, which facilitates the biomedical applications with low toxicity. We studied *in vitro* photothermal cell-killing efficacy of HA-PANI NPs by MTT assay and confocal microscopy measurement. The results reveal that HA-PANI NPs can selectively kill the cancer cells of HeLa and HCT-116 cells rather than normal cells of HFF cells upon exposure to a NIR 808 nm laser. The efficient intracellular intake of the HA-PANI NPs by both HeLa and HCT-116 cells are observed, confirming their targeted ability for CD44-overexpressing cancer cells. Furthermore, the results of *in vivo* photothermal ablation of tumor show excellent treatment efficacy, indicating that the HA-PANI NPs can be considered as an extremely promising nanoplatform for targeted PTT of cancer.

Introduction

The photothermal therapy (PTT), a hyperthermia treatment that is achieved through the conversion of energy absorbed from particular photons by PTT agent into heat energy, can cause damage and even death of cancer cells by heating tumor tissue for minutes, which has been a research hotspot in the forefront of medical science and materials science due to its unique advantages such as remote controllability and low systemic toxicity, compared with traditional therapy techniques, such as surgery, chemotherapy, and radiotherapy.[1–5] As a result, the design and study of nanomaterials suited for PTT ablation of cancer has received ever-increasing attention, where a variety of nanomaterials with remarkable optical absorbance in the tissue-transparent near-infrared (NIR) window (700–900 nm), have been widely explored as photothermal agents by a large number of research groups.[1,3,6–10] Nevertheless, most of these currently used PTT agents were inorganic nanomaterials, such as gold-based nanomaterials,[1,11–13] carbon nanomaterials,[14–18] palladium nanosheets,[19] copper sulfide and copper selenide nanoparticles,[20,21] which are non-biodegradable and usually would remain in the body for long periods of time with long-term metal bioaccumulation.[22,23] Thereby, organic photothermal agents, typically polymeric ones with outstanding biocompatibility, have attracted widespread interest for PTT applications.[3,22,24–27]

Polyaniline (PANI) is the oldest and potentially one of the most useful conducting polymers.[28–30] A unique feature of PANI is that it can switch from the emeralidine base (EB) to the emeralidine salt (ES) by doping acids, transition metals, alkali ions and so on, which can lead to high conductivity and strong NIR absorption.[6] Recent studies have showed that the absorption of NIR light for PANI can generate a substantial amount of heat energy, and thus it can serve as promising photothermal agent.[6,25,31] One kind of ES PANI nanoparticles (PANI NPs) caped with PEGylated fatty acid has been synthesized, showing NIR photothermal property depended on the pH value in the presence of oxidative species of intracellular

environment.[6] The poly(N-vinylpyrrolidone)-modified PANI NPs were applied to evaluate the *in vivo* efficacy of photothermal therapy in a tumor-bearing mice model.[31] Pluronic F127-modified PANI NPs for photothermal ablation of tumor has been performed, which further demonstrated that PANI materials can act as a platform technology for the next generation of PTT agents.[25] In such studies, the addition of stabilizers and dopants, including of PEGylated fatty acid, poly(N-vinylpyrrolidone) and pluronic F127, has successfully overcome several obstacles for applications of PANI in PTT, *e.g.* water solubility and NIR photothermal conversion efficiency. However, function of these PANI NPs is considerably single, only pursuing monofunctional PTT, which is lack of adding other functionalities intended to improve delivery, therapeutic efficacy, and ultimately patient outcome.[6,25,31] The design and development of multifunctional therapeutic nanoplatforms, especially with targeted specificity, are considered necessary for future use in clinical cancer treatment,[32] because the intrinsic toxicity of treatment agents is inevitable to induce the damage of normal human tissues.[32–34] Along with this idea, Haam and co-workers in 2014 developed one kind of targeted gadolinium-enriched PANI NPs via modification of cetuximab, where they achieved simultaneous diagnostic imaging and PTT of epithelial cancer.[35] Despite the encouraging results gained, the relatively complex steps are needed for the preparation.[35] Thus, it will still be of great interest and importance to construct PANI-based PTT nanoplatforms with highly targeted specificity through facile methods.

Hyaluronic acid (HA), a kind of water-soluble and acidic polysaccharides with negatively charged, plays important roles in many biological functions as one of the components of extracellular matrix.[36,37] One unique feature of HA lies in the active targeting toward tumor cells through selectively binding specific receptors, such as CD44, which are abundantly overexpressed on the surface of various tumor cells.[38–40] Such an interesting selectivity of HA to CD44 has shown great potential application in biomedical fields, including drug delivery,[41–43] gene delivery[44,45] and imaging.[46,47] Beyond this, it has recently been reported that HA can be used to conjugate with water-insoluble nanomaterials, such as organic polymer[48] and carbon nanomaterials,[43,49–51] offering them good solubility for bioapplications. In view of the above-mentioned characteristics of HA, the combination of HA with PANI is a promising method to fabricate water-soluble multifunctional HA-PANI hybrid for PTT.

Building from these ideas, we herein attempt to fabricate one kind of water-soluble HA-hybrided PANI NPs (HA-PANI NPs) by one-step oxidative polymerization of aniline using HA as stabilizer in aqueous medium, where non-covalently electrostatic interaction between the negatively charged polymer HA and the cationic polymer PANI drives the formation of HA-PANI NPs. Benefitting from the photothermal feature of PANI and the targeted specificity of HA, HA-PANI NPs may be endowed with highly targeted PTT of cancer. This remarkably multifunctional property makes HA-PANI NPs can be considered as an extremely promising nanoplatform for biomedical application.

Results and Discussion

Synthesis and characterization of HA-PANI NPs. HA-PANI NPs are nanohybrids, which were fabricated through self-assembly of the negatively charged polymer HA and the cationic polymer PANI (Scheme 1). PANI is primarily polymerized from aniline monomer by one-step oxidative polymerization using ammonium peroxydisulfate (APS) as oxidant in aqueous medium without any acid. Meanwhile, anionic stabilizer HA twists the as-synthesized PANI by electrostatic interaction and then they roll together into random NPs. As a control, PANI was also synthesized according to the procedure for synthesis of HA-PANI NPs in the absence of HA. An intuitive comparison between PANI and HA-PANI NPs is represented (Fig. 1b). PANI are scarcely dispersed in water, whereas the as-prepared HA-PANI NPs exhibit considerable water-solubility with a dark green color, which can remain stable in aqueous solution for more than eight weeks at room temperature without any aggregation. This significant difference in solubility of PANI and HA-PANI NPs implies that PANI modified with HA are successfully achieved in HA-PANI NPs.

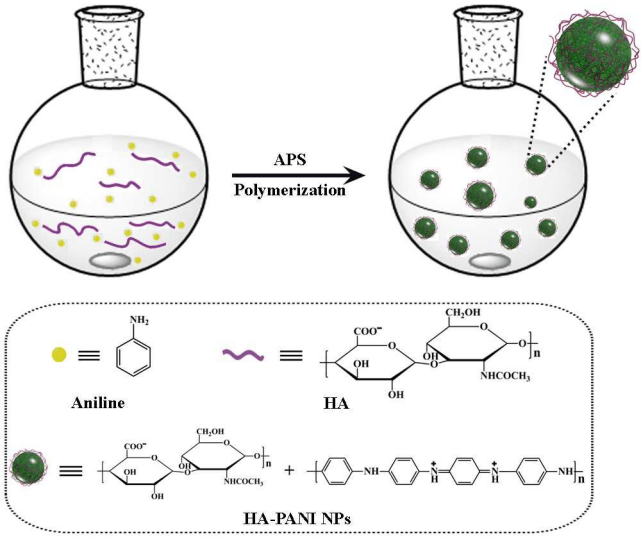

Scheme 1 Schematic illustration of preparation of HA-PANI NPs (counterions are omitted for clarity).

Furthermore, HA-PANI NPs were detailedly characterized by electron microscopy measurement, Fourier transform infrared (FT-IR) spectroscopy and thermogravimetric analysis (TGA). Scanning electron microscopy (SEM) measurement was performed to examine morphology and size distribution of PANI and HA-PANI NPs. SEM image shows that HA-PANI NPs have uniform spherical shape with a diameter around 40 nm and are well separated from each other (Fig. 1c and Fig. S1). By contrast, PANI are massive aggregates (Fig. 1a) with insolubility in water (Fig. 1b), which is consistent with the previous report.[52] Meanwhile, atomic force microscopic (AFM) measurement was also employed to investigate morphology of HA-PANI NPs (Fig. 1e), giving similar result to that of SEM measurement. Dynamic laser scattering (DLS) and zeta potential measurements were further carried out to identify the

HA-PANI NPs size and surface charged distribution (Fig. 1d, Fig. S2 and S3). The corresponding average hydrodynamic diameter of HA-PANI NPs is 98 nm with a sharp size distribution (Fig. 1d and Fig. S2). The result implies HA-PANI NPs with a uniform size distribution, in well agreement with the results of SEM and AFM measurements. The hydrodynamic diameter is larger than the SEM determined diameter. This is because DLS measures the size of the particles together with solvent molecule.[53] Zeta potential analysis gives potential values of +10.2 mV for PANI and –27.5 mV for HA-PANI NPs (Fig. S3), revealing PANI with positive charge and HA-PANI NPs with negative charge. The opposite electrical properties of PANI and HA-PANI NPs illustrates that negatively charged HA exists on the surface of cationic PANI backbone in HA-PANI NPs. These facts confirm that uniform spherical nanoparticles are successfully synthesized, and also interpret different solubility of PANI and HA-PANI NPs, where PANI complexed with HA are relatively small-size and stable in the aqueous phase, benefitting from that the outstanding hydrophilicity of negative charged HA on the surface of PANI avoids the further aggregation of PANI. In addition, the sizes of HA-PANI NPs (about 100 nm) are suited for further biological applications.

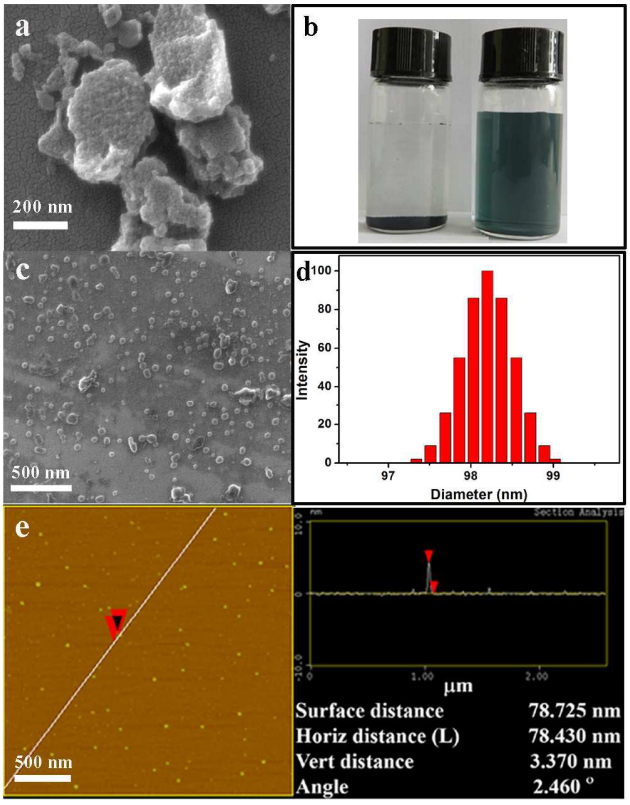

Fig. 1 (a) SEM image of PANI; (b) photographs of PANI (left) and HA-PANI NPs (right) dispersed in water; SEM image (c), hydrodynamic diameter distribution (d) and AFM image (e) of HA-PANI NPs.

Subsequently, FT-IR spectroscopy was employed to characterize the chemically structural feature of HA-PANI NPs (Fig. 2). All typical characteristic peaks of the HA-PANI NPs are shown in the range of 4000–400 cm^{-1}. The bands at 1583 and 1504 cm^{-1} can be assigned to the C=N and C=C stretching vibration of the quinoid and benzenoid rings of PANI. The band at 1301 cm^{-1} is due to C–N stretching mode for the secondary aromatic amine. The bands at 1147 and 828 cm^{-1} can be attributed to the vibration of the $–NH^{+}=$ structure and the out-of-plane deformation of C–H in the 1,4-disubstituted benzene ring, respectively. Besides these characteristic bands due to vibration of PANI, the bands at 1415 and 1045 cm^{-1}, assigned to carboxylate symmetric stretching and C–O–C stretching vibration of HA skeleton, can also be clearly found in the FT-IR spectrum. It should be noted that a band assigned to carboxylate asymmetric stretching vibration of HA should be expected somewhere near 1617 cm^{-1}; however, it is overshadowed by the stronger C=N band of PANI, and, therefore, it could not be resolved. These observations well agree with the previously reported results,[54–56] which further verify the successful combination of PANI with HA in HA-PANI NPs. Moreover, compared with PANI alone, the characteristic bands at 1578 and 1143 cm^{-1}, assigned to the vibration of the C=N and $–NH^{+}=$ structure, are slightly shifted to 1583 and 1147 cm^{-1} in HA-PANI NPs, respectively. Meanwhile, the band at 1409 cm^{-1} in HA, attributed to the carboxylate symmetric stretching of HA skeleton, is shifted to 1415 cm^{-1}. Such changes can be ascribed to the electrostatic interaction between carboxyl group of HA and ammonium group of PANI. This result demonstrated our foregoing hypothesis that the electrostatic self-assembly drives the formation of HA-PANI NPs.

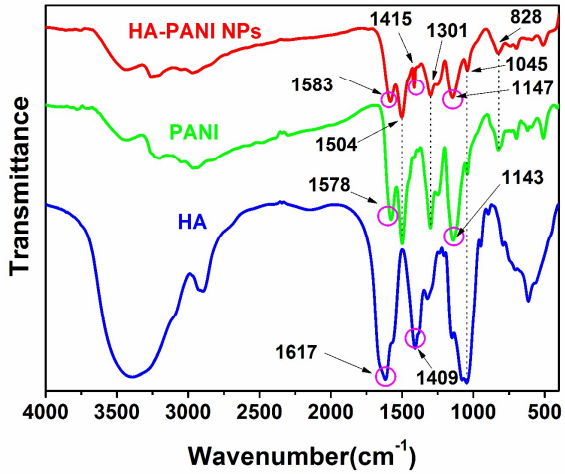

Fig. 2 FT-IR spectra of HA, PANI and HA-PANI NPs.

To give insight into the each quantity of HA and PANI in HA-PANI NPs, TGA was performed (Fig. 3). The curve of PANI exhibits two discrete weight losses from 25 to 620 °C and a total loss of weight of about 39%, which may correspond to the loss of water and the degradation of the PANI, respectively. A loss of weight of 87% is observed for HA in characteristic thermogram results. The first loss of weight occurs before 120 °C, which may be related to the adsorbed water. A sharp reduction of weight is recorded between 220 and 280 °C (Fig. 3), attributed to the decomposition of HA. Then, the sample weight decreases gradually. Similar steps of weight loss are reported in the literature.[56] It is detected from the thermograms that HA-PANI NPs presents some similarities to that of PANI but a little slower rate of weight loss (Fig. 3). From the

weight residue quantity at 900 °C, the each quantity of HA and PANI in HA-PANI NPs was calculated, where HA-PANI NPs are composed of 16% HA and 84% PANI.

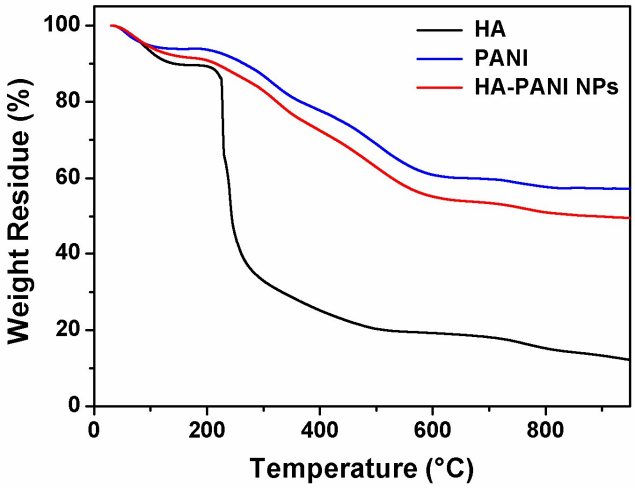

Fig. 3 TGA curves of HA, PANI and HA-PANI NPs under N_2 atmosphere.

Photothermal properties of HA-PANI NPs. PANI has strong optical absorption in the NIR region and can convert NIR light to a substantial amount of heat energy, which make PANI ideal for use as photothermal agent with absorbing NIR light.[6,25,31] Before studying photothermal feature of HA-PANI NPs, it is important to evaluate their absorption property. A comparison of PANI and HA-PANI NPs in DMSO was primarily carried out.[57] As seen from UV–Vis–NIR spectra (Fig. 4), it can be found that for PANI, two absorption bands at 430 and around 670 nm are observed, assigned to π–π transition of the benzene rings and charge transfer between quinoid and benzenoid rings, respectively. Relative to PANI, the band due to π–π transition of HA-PANI NPs is not observed, and the band attributed to charge transfer between quinoid and benzenoid rings appears at 668 nm, close to the absorption peak of PANI. It indicates that no doping process of PANI in HA-PANI NPs occurs like PANI alonely, referring to the previous studies.[6,58] Notedly, for HA-PANI NPs in water, the band assigned to charge transfer between quinoid and benzenoid rings shows a substantial red shift, shifted to the NIR region with broad absorption peak centered at about 810 nm (Fig. 4). This change can be ascribed to existence of ES state as a result of PANI doped, which induces the movement of electrons and decreases the excitation-energy level, similar to the previous reports.[6,58] Such obviously difference of UV–Vis–NIR spectra of HA-PANI NPs in DMSO and water can be owing to the deprotonation of the imine sites of PANI in DMSO,[59–61] resulting in the occurrence of dedoped process in HA-PANI NPs, because of DMSO with slight alkalinity compared to water. Overall, as already reported studies that an ideal PTT material should fulfill adsorption of NIR light in the range of 700–900 nm that does not cause damage of blood or normal tissue,[62,63] we can infer that HA-PANI NPs in water maybe well-suited to become one kind of promising photothermal agent.

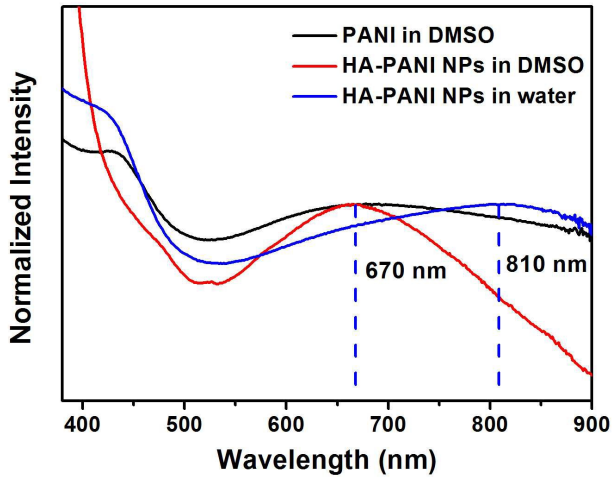

Fig. 4 UV–Vis–NIR spectra of PANI in DMSO and HA-PANI NPs in DMSO as well as water at 25 °C, normalized at 670 for PANI, 668 nm for HA-PANI NPs in DMSO, and 810 nm for HA-PANI NPs in water, respectively.

To verify the hyperthermic potential of HA-PANI NPs, we further recorded the temperature variations of HA-PANI NPs in aqueous solution upon exposure to a laser with a center wavelength of 808 nm and a power density of 2 W cm^{-2} by using a thermal imaging camera. As shown in Fig. 5b and 5c, the thermal signals of pure water show no significant temperature change ($\Delta T < 5$ °C) when exposed to laser light, indicating that no significant photothermal conversion occurs. On the contrary, the colors of photothermal images of the HA-PANI NPs solution continuously change from black (corresponding to low temperature) to bright red (corresponding to high temperature) with increasing exposure time (Fig. 5a), revealing a significant temperature raise from 23.8 to 63.9 °C in 10 min ($\Delta T = 40.1$ °C) (Fig. 5c). Such observation illustrates that the HA-PANI NPs can efficiently convert the 808 nm laser energy into thermal energy, which offers the possibility to proceed biomedical applications as PTT agent for cancer cell killing.

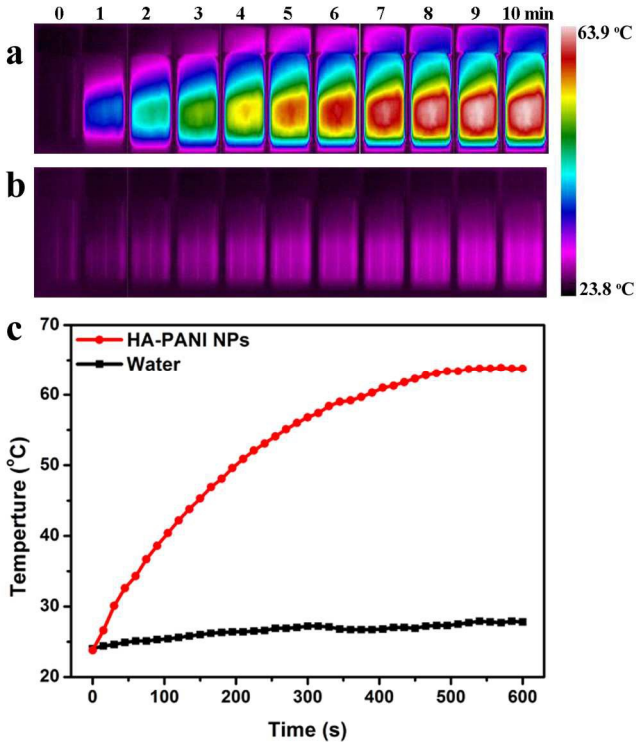

Fig. 5 Photothermal images of HA-PANI NPs solution (100 μg mL^{-1}) (a), and pure water (b) upon exposure to 808 nm laser (2 W cm^{-2}) for different time periods. (c) The corresponding time-dependent photothermal curves of samples.

Targeted photothermal cell-killing efficacy of HA-PANI NPs *in vitro*. We selected three kinds of cells to examine the dark cytotoxicity and the photothermal cell-killing efficacy of HA-PANI NPs *in vitro*. The normal cell used there is human foreskin fibroblasts (HFF) cells which is low CD44 expression.[64] The cancer cells are human colon cancer (HCT-116) cells and human cervix cancer (HeLa) cells with high CD44 expression.[33,39,44,65] Prior to exploiting the photothermal cell-killing efficacy of HA-PANI NPs, it is crucial to first assess the stability of HA-PANI NPs in various physiologic solutions. From Fig. 6a, it is found that HA-PANI NPs can be persevered in water, 0.9% NaCl aqueous solution, phosphate buffered saline (PBS) and Dulbecco's modified eagle medium (DMEM) without any aggregation, which confirms the excellent solution-stability of HA-PANI NPs. Additionally, as a potential PTT agent, the dark cytotoxicity of HA-PANI NPs was assessed at different concentrations of HA-PANI NPs from 0 to 100 μg mL^{-1} for 24 h by standard MTT assay. As shown in Fig. 6b, all cell viabilities of over 85% are observed, even at the high concentration of 100 μg mL^{-1}. These data exhibit HA-PANI NPs have negligible cytotoxicity *in vitro*, which are suited to further exploit the photothermal therapeutic efficacy.

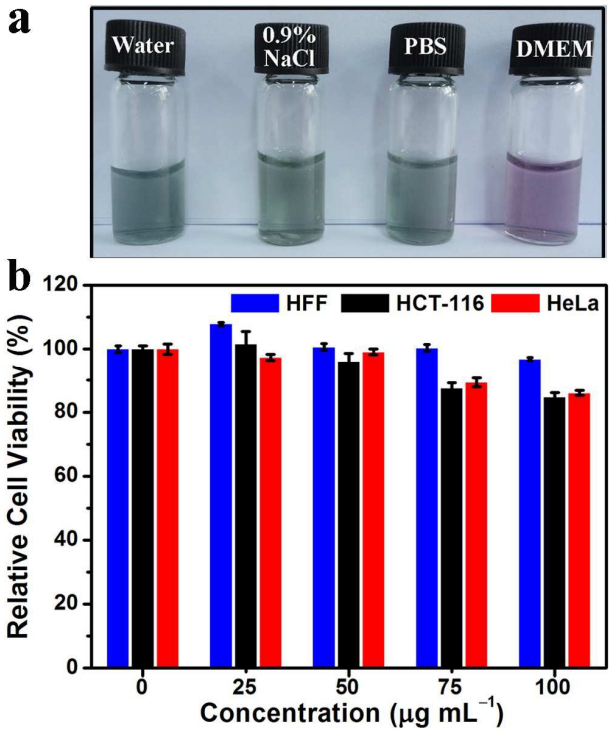

Fig. 6 (a) Photographs of HA-PANI NPs in water, 0.9% NaCl, PBS and DMEM. (b) *In vitro* cell viability of HFF, HCT-116 and HeLa cells incubated with HA-PANI NPs solutions with different concentrations from 0 to 100 μg mL^{-1} for 24 h, respectively.

To evaluate the photothermal cell-killing efficacy of HA-PANI NPs, we further performed *in vitro* cytotoxicity experiments of HA-PANI NPs upon NIR irradiation. HFF, HCT-116 and HeLa cells were incubated in culture medium containing series of concentrations of HA-PANI NPs for 24 h, and then irradiated with 808 nm laser for 5 min, respectively. As shown in Fig. 7, for HFF cells, laser irradiation shows no apparent change in cell viability. The cell viabilities were higher than 89% even at the high concentration of HA-PANI NPs (100 μg mL^{-1}). In contrast, irradiation leads to decrease in the cell viabilities of HCT-116 and HeLa cells, which are remarkably reduced from about 75 to 25% for HCT-116 cells and 69 to 33% for HeLa cells with increase in the concentrations of HA-PANI NPs from 25 to 100 μg mL^{-1} (Fig. 7), showing concentration-dependent cell-killing efficacy. These results indicate that HA-PANI NPs can more effectively destroy HCT-116 and HeLa cells than HFF cells upon NIR laser irradiation, which exhibits distinguished selectivity for photothermal cell-killing. Such obviously targeted specificity may be ascribed to the overexpression of HA receptors on the cell surface of HCT-116 and HeLa cells, similar to other HA-targeted systems.[33,44] Moreover, as a control, without HA-PANI NPs, laser irradiation shows nearly no damage of all kinds of cells (Fig. 7). An attempt was made to perform the cell viability experiment of PANI with irradiation, but was restricted, because of its insolubility in aqueous solution.

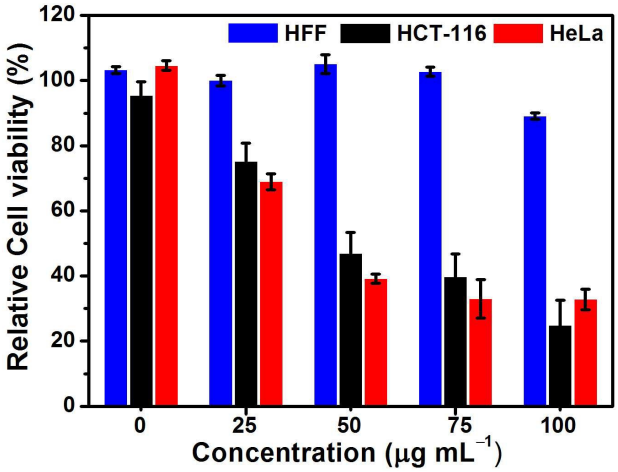

Fig. 7 Photothermal cell killing. HFF, HCT-116 and HeLa cells were incubated with HA-PANI NPs solutions with different concentrations from 0 to 100 μg mL^{-1} for 24 h at 37 °C , and then irradiated by a 808 nm laser (2 W cm^{-2}) for 5 min.

Confocal microscopy measurement was also performed to evaluate *in vitro* therapeutic efficacy of HA-PANI NPs upon irradiation, where calcein-AM and propidium iodide (PI) were used for identifying living cells and dead cells, respectively.[66–68] HFF, HCT-116 and HeLa cells were incubated with HA-PANI NPs for 24 h, and then treated with calcein-AM and PI. The confocal microscopy images are acquired before irradiation. The calcein-AM fluorescence (green) is observed in each kind of cells, and no PI fluorescence (red) is detected (Fig. 8A), indicating that cells were not damaged by HA-PANI NPs in the absence of NIR irradiation. After exposed to the 808 nm laser for 15 min, an intense fluorescent signal of PI is observed from the HCT-116 and HeLa cells, whereas for HFF cells, no PI fluorescence was still observed (Fig. 8B). Merging the fluorescent images reveals that the fluorescence of PI is originated from the intracellular region (Fig. 8C). Meanwhile, the morphological changes, such as cell-membrane shrinking, are clearly observed in HCT-116 and HeLa cells after irradiation, showing that HA-PANI NPs can induce obvious apoptosis in cells. Such results illustrate that HA-PANI NPs can selectively kill HCT-116 and HeLa cells rather than HFF cells upon exposure to a NIR laser, in accordance with MTT assay (Fig. 7).

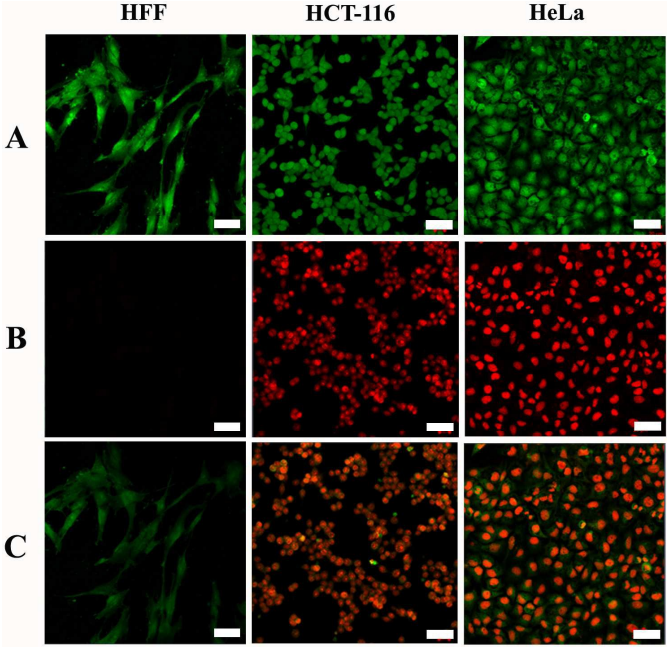

Fig. 8 Confocal microscopy images of HFF, HCT-116 and HeLa cells stained with calcein-AM (green, living cells) and PI (red, dead cells), using a 20 × objective lens, respectively. The cells were cultured with HA-PANI NPs (100 μg mL^{-1}): (A) before irradiation; (B) after irradiation; (C) merged images. Scale bar: 40 μm.

To further confirm the targeted specificity of HA-PANI NPs towards HCT-116 and HeLa cells nor HFF cells, the cells were treated with HA-PANI NPs for different time, and then monitored cellular uptake of HA-PANI NPs through analysis of the UV–Vis–NIR intensity at 810 nm, in which the absorption of cells themselves can be excluded.[69] As shown in Fig. 9, for HFF cells, the absorption intensity is almost unchanged with raising time. However, for HCT-116 and HeLa cells that own the HA receptor, the absorption intensity gradually increases as time goes, and then reaches a plateau at the time of > 60 and 120 min for HeLa and HCT-116 cell. If cellular uptake is receptor-mediated, along with the raise of incubation time, the HA-PANI NPs will efficaciously accumulate inside cells and the absorption intensity at 810 nm will increase. Thus, the result indicates that the cellular uptakes of HA-PANI NPs for HCT-116 and HeLa cells are receptor-mediated. Based on this result and given that HA can effectively bind CD44 and CD44 are overexpressed on the surface of HCT-116 and HeLa cells,[33,65,66] we can deduce that the hydrophilic HA of HA-PANI NPs specifically recognizes HCT-116 and HeLa cells by strongly binding to CD44 on the cell surface, and then they enter cells through receptor-mediated endocytosis. Further laser irridiation leads to heating of HA-PANI NPs endocytosed and killing for these cells, which well agrees with the results of MTT assay (Fig. 7) and confocal microscopy (Fig. 8) that HA-PANI NPs can selectively kill HCT-116 and HeLa cells rather than HFF cells upon exposure to a NIR laser. This targeted specificity makes HA-PANI NPs can be considered as an extremely promising candidate for cancer therapeutics through photothermal killing.

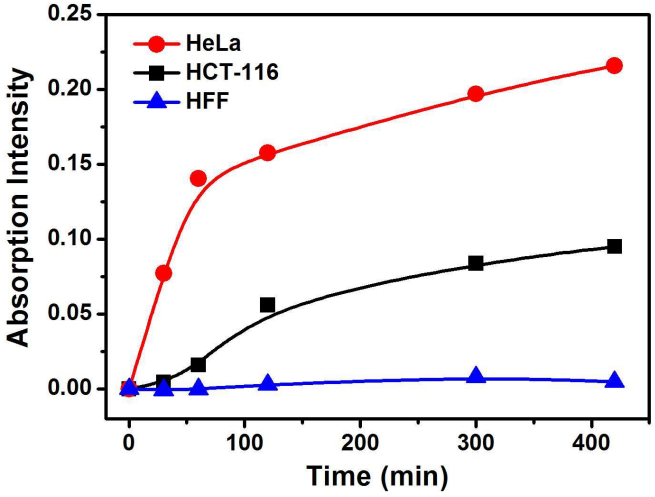

Fig. 9 Time-dependent absorption curves at 810 nm of HA-PANI NPs accumulated inside HFF, HCT-116 and HeLa cells at different incubation time from 0 to 420 min, respectively.

PTT of cancer *in vivo*. Finally, the HA-PANI NPs-induced PTT of cancer in vivo was further studied using four groups of female Balb/c nude mice bearing HeLa cancer cells. In the test group (HA-PANI NPs + Laser), a saline solution of HA-PANI NPs was injected into the tumor site and exposed to a 808 nm laser irradiation at a power density of 0.64 W cm^{-2} for 5 min. For comparison, mice without injection of HA-PANI NPs (Laser only) and without exposure to the 808 nm laser (HA-PANI NPs only) were used as the control groups, respectively; untreated mice, with neither injection of HA-PANI NPs nor 808 nm laser exposure, were chosen as the blank group (Blank). Tumor sizes were monitored every day after treatment (Fig. 10). The tumors of the test group shrink during the first five days. On the sixth day, the tumors are completely eliminated, with only scars left at the original tumor site (Fig. 10). In marked contrast, tumors in the control and the blank groups show rapid growth. These results demonstrate that only NIR laser irradiation or HA-PANI NPs injection do not affect tumor development, in good agreement with the result evaluated by experiments *in vitro*. Body weight change is also an important indicator for evaluating the potential *in vivo* toxicity of NPs. The body weight of mice was recorded over a 14-day period (Fig. S4). During the first 5 days, the body weight of the test group decreases rapidly compared with that of the mice in the blank group, probably owing to tumor shrink induced by the PTT treatment. Afterwards, the body weight begins to increase, and small weight differences between the test and blank group are observed by day 14. The fluctuation in body weight shows a similar tendency to that of the relative tumor volume, indicating no obvious signs of toxic effects after PTT treatment. These observations well agree with the previously reported results,[25] which indicate the excellent efficacy of *in vivo* PTT of cancer using HA-PANI NPs. Nevertheless, much more effort, including their accumulation and distribution in tumor tissues and all major organs, targeted specificity *in vivo*, is needed to be further made for exploring the potential applications of HA-PANI NPs.

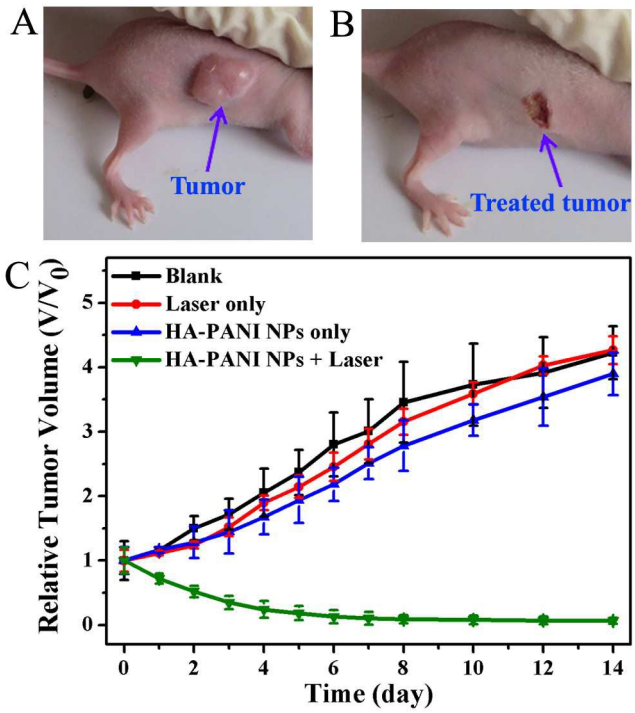

Fig. 10 *In vivo* PTT study. Representative photographs of tumor with injection of HA-PANI NPs before (A) and after (B) 808 nm irradiation (0.64 W cm^{-2}) on the sixth day. (C) Tumor growth rates of groups after different treatment. A saline solution of HA-PANI NPs was injected into the tumor site and exposed to 808 nm laser (HA-PANI NPs + Laser, $n = 3$). Mice with no injection of HA-PANI NPs (Laser only, $n = 3$) or without 808 nm laser exposure (HA-PANI NPs only, $n = 3$); blank group with neither injection of HA-PANI NPs nor 808 nm laser exposure (Blank, $n = 3$).

Conclusions

In conclusion, the water-soluble HA-hybrided PANI NPs (HA-PANI NPs) have been successfully prepared by one-step oxidative polymerization using aniline as polymerized monomer and HA as a stabilizer and targeted agent, where non-covalently electrostatic interaction between the negatively charged polymer HA and the cationic polymer PANI drives the formation of HA-PANI NPs. The as-prepared HA-PANI NPs with suitable nanosize (average hydrodynamic diameter around 100 nm) can efficiently convert the 808 nm laser energy into thermal energy. Besides, HA-PANI NPs have negligible cytotoxicity *in vitro*, which facilitates the biomedical applications with low toxicity. Furthermore, the results of *in vitro* cell viability reveal that HA-PANI NPs can selectively kill CD44-mediated cancer cells rather than normal cells via exposure to a NIR 808 nm laser. The efficient intracellular targeted intake of the HA-PANI NPs by both HeLa and HCT-116 cells are observed, indicating their targeted ability for CD44-overexpressing cancer cells. Furthermore, *in vivo* photothermal ablation of tumor with excellent treatment efficacy was achieved. Taken together, these results highlight that HA-PANI NPs can be considered as an extremely promising nanoplatform for targeted PTT of cancer.

Experimental section

Materials

Aniline was purchased from Aladdin Reagent Company (Shanghai, China). Ammonium peroxydisulfate (APS) and dimethylsulfoxide (DMSO) were obtained from Xilong Chemical Corporation (Guangdong, China). Hyaluronic acid (HA) was purchased from Freda Company (Shandong, China). DMEM medium (high glucose) was obtained from Gibco Company (USA). Fetal bovine serum was obtained from HyClone Company (USA). 0.25% Trypsin was obtained from Auki Biological Company (Jinan, China). Penicillin-streptomycin, phosphate-buffered saline tablet (PBS), propidium iodide (PI) and 3-(4,5-dimethylthiazolyl-2)-2,5-diphenyltetrazolium bromide (MTT) were purchased from Sigma Company (USA). Calcein-AM was obtain from Invitrogen (Shanghai, China). Human cervical carcinoma cells (HeLa), human colon cancer cells (HCT-116) and human foreskin fibroblasts (HFF) were supplied from Immunetech International (Guilin, China). All solvents and reagents were of analytical grade and used without further purification. Water was purified with a Milli-Q apparatus (Millipore, Bedford, MA).

Synthesis of HA-PANI NPs.

Referring to the synthetic method of PANI without HA reported by Mohamad *et al*,[52] water-soluble HA-hybrided PANI NPs (HA-PANI NPs) were synthesized, described as follows: HA (1.63 g) and aniline (0.65 g) were mixed in 30 mL deionized water. The mixture was well-stirred for 20 min at room temperature. Subsequently, 1.60 g APS in deionized water (70 mL) was slowly added for 1 hour under ice-water bath. The reaction mixture was stirred for another 24 h under ice-water bath, and dark-green precipitate formed. After warming up to room temperature, the resulting precipitate was filtered, washed with a small amount of water to remove inorganic salts and reactants, and dried in a vacuum to obtain dark-green power.

Characterizations.

UV–Vis–NIR spectra were collected from 250–900 nm by Lambda 45 UV–Vis–NIR spectrophotometer (Perkin Elmer, USA). The Fourier transform infrared (FT-IR) spectra were obtained on a Perkin Elmer FT-IR spectrometer. Thermogravimetric analysis (TGA) was performed on *LABSYS evo* thermogravimetric analyzer under nitrogen atmosphere with a heating rate of 10 °C min^{-1} up to 900 °C. Scanning electron microscopy (SEM) experiments were performed on FEI Quonta 200 FEG. Atomic force microscopy (AFM) experiment was performed on di NanoScope IVa Controller, Vecco, USA. Dynamic laser scattering (DLS) experiment was carried on a laser light scattering spectrometer (BI-200SM) equipped with a digital correlator (BI-9000AT) at 532 nm. Zeta potential measurement was carried out on Malvern Zetasizer Nano ZS-90.

Photothermal imaging of HA-PANI NPs.

The photothermal images of pure water and HA-PANI NPs in aqueous solution were taken by Infrared camera (MAG30, Magnity Electronics, China) in conjunction with the 808 nm laser. The aqueous solution of HA-PANI NPs (100 μg mL^{-1}) was placed in a specimen bottle and irradiated by 808 nm laser (2 W cm^{-2}). The temperature signals recorded at different time intervals (0~10 min) were analyzed with Magnity Electronics tools systems. Under the same condition, the efficacy of pure water was also studied.

Cell culture.

The HFF, HCT-116 and HeLa cells were cultured in RPMI-DMEM medium containing with 10% fetal bovine serum (FBS) and 1% penicillin-streptomycin, incubated at 37 °C under a 5% CO_2 atmosphere, respectively.

The cytotoxicity of HA-PANI NPs.

The cytotoxicity of HA-PANI NPs was measured by MTT assay on HFF, HCT-116 and HeLa cell lines. The cells were seeded in a 96-well cell culture plate at a density 1×10^4 cells/100 μL per well at 37 °C under a 5% CO_2 for 24 h. 100 μL of HA-PANI NPs (0, 50, 100, 150, 200 μg mL^{-1}) were added to per well for 24 h. Thereafter, the MTT reagent (10 μL in PBS, 5 mg mL^{-1}) was added to each well for another 4 h to test the cytotoxicity through Infinite M1000. The cytotoxicity was expressed as the percentage of cell viability compared to that of untreated control cells.

The photothermal therapy effect of HA-PANI NPs.

The photothermal therapy effects of HA-PANI NPs were also taken by MTT assay on HFF, HCT-116 and HeLa cell lines. The cells were also incubated with HA-PANI NPs (0, 25, 50, 75, 100 μg mL^{-1}) on 96-well plates for 24 h, containing 1×10^4 cells/200 μL in each well. After that, an 808 nm laser (2 W cm^{-2}) was used to irradiate cells for 5 min. The resulting cells were incubated for additional 24 h. Then, the MTT reagent (10 μL in PBS, 5 mg mL^{-1}) was added into the cells for another 4 h to test the photothermal therapy effect by Infinite M1000.

Confocal microscopy measurement.

Confocal microscopy (Carl Zeiss LSM 710, Jena, Germany) was used to observe the target and photothermal therapy effects of HA-PANI NPs for HFF, HCT-116 and HeLa cells. Briefly, HFF, HCT-116 and HeLa cells were seeded into 24-well microplates at a density 2×10^4 cells mL^{-1} per well and cultured at 37 °C under a 5% CO_2 atmosphere for 24 h, respectively. 1 mL fresh medium containing 100 μg mL^{-1} HA-PANI NPs was added into each well for another 24 h. The medium was discarded, and the cells was washed by PBS for 3 times to remove the unbound HA-PANI NPs. 1 mL fresh medium was added again. A 808 nm laser (2 W cm^{-2}) was used to irradiate cells for 15 min, and the cells were stained with calcein-AM (1.6%) and PI (2%) for 10 minutes before and after irradiation. Then, conforcal images were taken before and after illumination using a 20 × objective lens.

UV–Vis–NIR intensity analysis of the HA-PANI NPs accumulation on HFF, HCT-116 and HeLa cells.

2 mL of HFF, HCT-116 and HeLa cells (a density of 2×10^4 cells mL^{-1} per well) were seeded in each well of 6-well plate and incubated overnight at 37 °C under 5% CO_2, respectively. Then, the cells were treated with HA-PANI NPs (100 μg mL^{-1}) in 2 mL of fresh medium for different incubation time (0, 30, 60, 120, 300, 420

min). Subsequently, cells were washed twice with PBS. After that, in order to collect cells, they were digested and centrifuged at 1,000 rpm for 3 minutes, and the as-obtained cells were disrupted by SCIENTZ-IID. Finally, the cellular uptake results of HA-PANI NPs were determined using UV–Vis–NIR spectrophotometer within a wavelength range 300–900 nm.

Photothermal therapy of cancer *in vivo*.

The animal protocol was conducted according to the Guideline for the Care and Use of Laboratory Animals (NIH publication 85-23), and was approved by the Experimental Animal Ethics Committee of Guangxi Medical University Laboratory Animal Centre (No. 20141224-XC). Female Balb/c nude mice that 5~6 weeks old were purchased from Beijing Vital River Laboratory Animal Technology Co. Ltd.(Beijing, China). HeLa tumor-bearing mice were established by subcutaneous injection of 1×10^7 cells suspended in physiological saline (200 μL) into the flank region of each nude mouse. The mice were used for phototherapeutic experiments, when the tumors reached an approximate size of 150 mm^3.

Test group: saline solution of HA-PANI NPs (50 μL, 4 mg/mL) was injected into the tumor site, and the mice were exposed to 808 nm laser (0.64 W cm^{-2}) for 5 min (HA-PANI NPs + Laser, n = 3). Control groups: mice without injection of saline solution of HA-PANI NPs (Laser only, n = 3) or without 808 nm laser exposure (HA-PANI NPs only, n = 3). Blank group: mice with no injection of saline solution of HA-PANI NPs and without 808 nm laser exposure (Blank, n = 3).

After the treatment, the sizes of the tumor were monitored every day and determined by the following equation: volume = (tumor length) × (tumor width)^2/2. Relative tumor volumes were calculated as V/V_0 (V_0 is the tumor volume when the treatment was initiated). The body weights of the mice were also monitored every day for 14 days. For the treatment, a group of 3 mice were used to assess the mean and standard deviation of the data.

Acknowledgements

This work was supported by the Natural Science Foundation of China (21161003 and 21364002), Guangxi Natural Science Foundation of China (2013GXNSFGA019001, 2012GXNSFDA053007 and 2014GXNSFBA118038), the Program for New Century Excellent Talents in University of the Ministry of Education (NCET-13-0743), the Program for New Century National Hundred, Thousand and Ten Thousand Talent Project of Guangxi, the State Key Laboratory Cultivation Base for the Chemistry and Molecular Engineering of Medicinal Resources (CMEMR2012-A12, CMEMR2013-A08 and CMEMR2013-A013), the Program for Guangxi Scientific Research of Higher Education (YB2014052), the Program for Key Scientific Research of Guangxi Normal University (2013ZD005). We thank Haihua Pan (Zhejiang University, China) for kind help with AFM test.

Notes and references

M*inistry of Education Key Laboratory for the Chemistry and Molecular Engineering of Medicinal Resources, College of Chemistry and Chemical Engineering, Guangxi Normal University, Guilin, 541004, P. R. China Tel: (+86) 773-5846273; E-mail: xcshen@mailbox.gxnu.edu.cn; hliang@gxnu.edu.cn*.

‡ Contributed equally to this work.

1 V. Shanmugam, S. Selvakumar and C.-S. Yeh, *Chem. Soc. Rev.*, 2014, **43**, 6254–6287.

2 S. Lal, S. E. Clare and N. J. Halas, *Acc. Chem. Res*., 2008, **41**, 1842–1851.

3 L. Xu, L. Cheng, C. Wang, R. Peng and Z. Liu, *Polym. Chem*., 2014, **5**, 1573–1580.

4 P. K. Jain, X. Huang, I. H. El-Sayed and M. A. El-Sayed, *Acc. Chem. Res*., 2008, **41**, 1578–1586.

5 Z. Qin and J. C. Bischof, *Chem. Soc. Rev*., 2012, **41**, 1191–1217.

6 J. Yang, J. Choi, D. Bang, E. Kim, E.-K. Lim, H. Park, J.-S. Suh, K. Lee, K.-H. Yoo, E.-K. Kim, Y.-M. Huh and S. Haam, *Angew. Chem. Int. Ed.*, 2011, **50**, 441–444.

7 H. Li, D. Chen, L. Li, T. Liu, L. Tan, X. Wu and F. Tang, *Angew. Chem. Int. Ed*., 2011, **50**, 891–895.

8 W. Li, R. Zamani, P. R. Gil, B. Pelaz, M. Ibáñez, D. Cadavid, A. Shavel, R. A. Alvarez-Puebla, W. J. Parak, J. Arbiol and A. Cabot, *J. Am. Chem. Soc*., 2013, **135**, 7098–7101.

9 A. Sahu, W. I. Choi, J. H. Lee and G. Tae, *Biomaterials*, 2013, **34**, 6239–6284.

10 B. Tian, C. Wang, S. Zhang, L. Feng and Z. Liu, *ACS Nano*, 2011, **5**, 7000–7009.

11 G. V. Maltzahn, J.-H. Park, A. Agrawal, N. K. Bandaru, S. K. Das, M. J. Sailor and S. N. Bhatia, *Cancer Res.*, 2009, **69**, 3892–3900.

12 S. Wang, K.-J. Chen, T.-H. Wu, H. Wang, W.-Y. Lin, M. Ohashi, P.-Y. Chiou and H.-R. Tseng, *Angew. Chem. Int. Ed*., 2010, **49**, 3777–3781.

13 J. Nam, N. Won, H. Jin, H. Chung and S. Kim, *J. Am. Chem. Soc.*, 2009, **131**, 13639–13645.

14 C. Wang, H. Tao, L. Cheng and Z. Liu, *Biomaterials*, 2011, **32**, 6145–6154.

15 F. Li, S.-J. Park, D. Ling, W. Park, J. Y. Han, K. Na and K. Char, *J. Mater. Chem. B*., 2013, **1**, 1678–1686.

16 M. Zhang, T. Murakami, K. Ajima, K. Tsuchida, A. S. D. Sandanayaka, O. Ito, S. Iijima and M. Yudasaka, *PNAS*, 2008, **105**, 14773–14778.

17 J. T. Robinson, S. M. Tabakman, Y. Liang, H. Wang, H. S. Casalongue, D. Vinh, and H. Dai, *J. Am. Chem. Soc*., 2011, **133**, 6825–6831.

18 T. Murakami, H. Nakatsuji, M. Inada, Y. Matoba, T. Umeyama, M. Tsujimoto, S. Isoda, M. Hashida and H. Imahori, *J. Am. Chem. Soc.*, 2012, **134**, 17862–17865.

19 X. Huang, S. Tang, X. Mu, Y. Dai, G. Chen, Z. Zhou, F. Ruan, Z. Yang and N. Zheng, *Nat. Nanotech*., 2011, **6**, 28–32.

20 Q. Tian, J. Hu, Y. Zhu, R. Zou, Z. Chen, S. Yang, R. Li, Q. Su, Y. Han and X. Liu, *J. Am. Chem. Soc*., 2013, **135**, 8571–8577.

21 Q. Tian, M. Tang, Y. Sun, R. Zou, Z. Chen, M. Zhu, S. Yang, J. Wang, J. Wang and J. Hu, *Adv. Mater*., 2011, **23**, 3542–3547.

22 L. Cheng, K. Yang, Q. Chen and Z. Liu, *ACS Nano*, 2012, **6**, 5605–5613.

23 S. Sharifi, S. Behzadi, S. Laurent, M. L. Forrest, P. Stroeve and M. Mahmoudi, *Chem. Soc. Rev.* 2012, **41**, 2323–2343.

24 K. Yang, H. Xu, L. Cheng, C. Sun, J. Wang and Z. Liu, *Adv. Mater*., 2012, **24**, 5586–5592.

25 J. Zhou, Z. Lu, X. Zhu, X. Wang, Y. Liao, Z. Ma and F. Li, *Biomaterials*,

2013, **34**, 9584–9592.
26 C. M. MacNeill, E. M. Wailes and N. H. Levi-polyachenko, *J. Nanosci. Nanotechnol.*, 2013, **13**, 3784–3791.
27 H. Gong, L. Cheng, J. Xiang, H. Xu, L. Feng, X. Shi and Z. Liu, *Adv. Funct. Mater*., 2013, **23**, 6059–6067.
28 D. Li, J. Huang and R. B. Kaner, *Acc. Chem. Res*., 2009, 42, 135–145.
29 A. J. Heeger, *Angew. Chem. Int. Ed*., 2001, **40**, 2591–2611.
30 J. Shi, Y. Chen, Q. Wang and Y. Liu, *Adv. Mater.* 2010, **22**, 2575–2578.
31 L. E. Ibarra, E. I. Yslas, M. A. Molina, C. R. Rivarola, S. Romanini, C. A. Barbero, V. A. Rivarola and M. L. Bertuzzi, *Laser Phys*., 2013, **23**. 066004.
32 Z. Cheng, A. A. Zaki, J. Z. Hui, V. R. Muzykantov and A. Tsourkas, *Science*, 2012, **338**, 903–910.
33 R. Chen, X. Wang, X. Yao, X. Zheng, J. Wang and X. Jiang, *Biomaterials*, 2013, **34**, 8314–8322.
34 Y. Akiyama, T. Mori, Y. Katayama and T. Niidome, *J. Control. Release*., 2009, **139**, 81–84.
35 T. Lee, D. Bang, Y. Park, S. H. Kim, J. Choi, Joseph Park, D. Kim, E. Kim, J.-S. Suh, Y.-M. Huh and S. Haam, *Adv. Healthcare Mater.,* 2014, **9**, 1408–1414.
36 J. L. Lapčík, L. Lapčík, S. D. Smedt, J. Demeester and P. Chabreček, *Chem. Rev.*, 1998, **98**, 2663–2684.
37 J. Entwistle, C. L. Hall and E. A. Turley, *J. Cell. Biochem.*, 1996, **61**, 569–577.
38 K. M. Park, J.-A. Yang, H. Jung, J. Yeom, J. S. Park, K.-H. Park, A. S. Hoffman, S. K. Hahn and K. Kim, *ACS Nano*, 2012, **6**, 2960–2968.
39 Y. Luo and G. D. Prestwich, *Bioconjugate Chem*., 1999, **10**, 755-763.
40 B. P. Toole, T. N. Wight, V. Disease and M. I. Tammi, *J. Biol. Chem*., 2002, **277**, 4593–4596.
41 Y. Yang, Y.-M. Zhang, Y. Chen, J.-T. Chen and Y. Liu, *J. Med. Chem*., 2013, **56**, 9725–9736.
42 H. Lee, K. Lee and T. G. Park, *Bioconjugate Chem*., 2008, **19**, 1319–1325.
43 H. Wu, H. Shi, Y. Wang, X. Jia, C. Tang, J. Zhang and S. Yang, *Carbon*, 2014, **69**, 379–389.
44 H. Lee, H. Mok, S. Lee, Y.-K. Oh and T. G. Park, *J. Control. Release*., 2007, **119**, 245–252.
45 G. Jiang, K. Park, J. Kim, K. S. Kim, E. J. Oh, H. Kang, S.-E. Han, Y.-K. Oh, T. G. Park and S. K. Hahn, *Biopolymers*, 2008, **89**, 635–642.
46 J. Li, Y. He, W. Sun, Y. Luo, H. Cai, Y. Pan, M. Shen, J. Xia and X. Shi, *Biomaterials*, 2014, **35**, 3666–3677.
47 D.-E. Lee, A. Y. Kim, G. Saravanakumar, H. Koo, I. C. Kwon, K. Choi, J. H. Park and K. Kim, *Macromol. Res*., 2011, **19**, 861–867.
48 A. Gelmi, M. J. Higgins and G. G. Wallace, *J. Phys. Chem. B.,* 2012, **116**, 13498–13505.
49 D. S. Kwag, K. Park, K. T. Oh and E. S. Lee, *Chem. Commun*., 2013, **49**, 282–284.
50 M. Swierczewska, K. Y. Choi, E. L. Mertz, X. Huang, F. Zhang, L. Zhu, H. Y. Yoon, J. H. Park, A. Bhirde, S. Lee and X. Chen, *Nano Lett.*, 2012, **12**, 3613–3620.
51 S. R. Datir, M. Das, R. P. Singh and S. Jain, *Bioconjugate Chem*., 2012, **23**, 2201–2213.
52 A. Mohamad, E.-H. Gad and Z. Sawsan, *Chem. Eng. J.*, 2013, **217**, 460–465.
53 B. Babić-Stojić, V. Jokanović, D. Milivojević, Z. JagliIić, D. Makovec, N. Jović and M. Marinović-Cincović, *J Nanomater*, 2013, **2013**, 741036.
54 Š. Ivana, T. Miroslava and S. Jaroslav, *Polym. Degrad. Stabil*., 2008, **93**, 2147–2157.
55 X.-R. Zeng and T.-M. Ko, *Polymer*, 1998, **39**, 1187–1195.
56 F. Sun and I. Zhitomirsky, *Surf. Eng*., 2009, **25**, 621–627.
57 PANI does not dissolve in water, and a comparison of PANI and HA-PANI NPs in water cannot be taken.
58 A. Gruger, A. E. Khalki and P. Colomban, *J. Raman. Spectrosc*., 2003, **34**, 438–450.
59 E. Dmitrieva and L. Dunsch, *J. Phys. Chem. B*, 2011, **115**, 6401–6411.
60 Y. Fu and R. A. Weiss, *Synth. Met.*, 1997, **84**, 103–104.
61 Y. Xia, J. M. Wiesinger and A. G. MacDiarmid, *Chem. Mater.,* 1995, **7**, 443–445.
62 W. R. Chen, R. L. Adams, R. Carubelli,and R. E. Nordquist, *Cancer Lett.* 1997, **115**, 25–30.
63 F. Helmchen and W. Denk, *Nat. Methods*, 2005, **2**, 932–940.
64 S. V. Smirnov, R. Harbacheuski, A. Lewis-Antes, H. Zhu, P. Rameshwar and S. V. Kotenko*, Virology*, 2007, **360**, 6–16.
65 M. Ma, H. Chen, Y. Chen, K. Zhang, X. Wang, X. Cui and J. Shi, *J. Mater. Chem.*, 2012, **22**, 5615–5621.
66 M. Qin, H. J. Hah, G. Kim, G. Nie, Y.-E. K. Lee and R. Kopelman, *Photoch. Photobio. Sci*., 2011, **10**, 832–841.
67 Z. Sheng, L. Song, J. Zheng, D. Hu, M. He, M. Zheng, G. Gao, P. Gong, P. Zhang, Y. Ma and L. Cai, *Biomaterials*, 2013, **34**, 5236–5243.
68 Y. Wang, K. Wang, J. Zhao, X. Liu, J. Bu, X. Yan and R. Huang, *J. Am. Chem. Soc*., 2013, **135**, 4799–4804.
69 P. Xu, J. Chen, Z. Chen, S. Zhou, P. Hu, X. Chen and M. Huang, *PloS One*., 2012, **7**, e37051.

Graphical Contents Entry

Water-soluble hyaluronic acid-hybrided polyaniline nanoparticles show effective photothermal ablation of cancer with targeted specificity.